

Treatment of Complex Configurations for Flutter Calculations

A.M.Rampurawala* and K.J. Badcock†,

*Computational Fluid Dynamics Laboratory,
Flight Sciences and Technology,
Department of Engineering,
University of Liverpool,
L69 3BX, United Kingdom.*

Keywords: CFD, computational aeroelasticity

The transfer between fluid and structural grids in an aeroelastic simulation is considered. A method for blending the transformation of different aircraft components is described. This method is also used to blend control surfaces into the wing or fin. Evaluation of this treatment is made against results obtained when the flap has a small gap at its ends. The integrity of the method has been tested by the successful application to a practical example of rudder buzz.

I. Introduction

Aeroelasticity based on Computational Fluid Dynamics (CFD) has advanced significantly in the past decade. Many of the practical issues for simulating complete aircraft have been overcome. This moves research on to a new plane where the exploitation of tools to predict and explain nonlinear aeroelastic phenomena is the focus. CFD based tools need to be applied to problems which feature significant aerodynamic nonlinearity to justify the cost of using a high level of flow modelling. This places the focus on problems with shock waves, vortices and flow separation.

There are at least three aeroelastic problems discussed in the literature which were or are candidates for a CFD based treatment. First, the B2 stealth bomber suffered uncommanded pitching oscillations during flight trials. An analysis based on CAP-TSD, structural modes and the flight control system was used to explain the behaviour.¹ Secondly, the F-16 has suffered limit cycle oscillations for certain store configurations. This has been simulated using RANS modelling by the US Air Force Research Laboratories² and the Dutch Aerospace Laboratory.³ Important contributory factors appear to be shock motions and separation. Thirdly, the F-18 has suffered fin buffet due to vortex breakdown in the vicinity of the vertical tails. Recent developments with Detached Eddy Simulation have allowed impressive simulations of the fin response.⁴ The simulation of these sorts of phenomena presents a challenge for CFD based aeroelastic methods and drives their development.

The starting point for the current work is the simulation of the aeroelastic behaviour of the Hawk trainer by CFD reported in reference.⁵ This work demonstrated the ability to conduct the simulation (and in particular to manage the transformation of information from the fluid grid to the structural grid and vice-versa), but as expected no significant nonlinear effects were present. In the current paper the issue of control surfaces is introduced and the opportunity is taken to further test the integrity of the CFD approach by referencing published data for the Goshawk aircraft.

*PhD student

†Professor, corresponding author. Tel. : +44(0)151 794 4847 , Fax. : +44(0)151 794 6841, Email : K.J.Badcock@liverpool.ac.uk

During its early development the T-45 (Goshawk) fighter trainer was reported to experience the phenomenon known as rudder buzz.⁶ A steady state and rigid CFD analysis was used to locate the shock waves that were thought to drive the buzz. However, to our knowledge no CFD based analysis has been published of the dynamic behaviour. This is a useful test of the CFD based analysis, improving confidence in the methods involved.

The particular case we consider is motivated by three flight tests of the T-45A development aircraft, representing the Hawk variant, now used by the US Navy. Rudder oscillations were described when flying at Mach 0.9 and 10,000 feet, Mach 0.95 and 20,000 feet, and at Mach 0.90 and 30,000 feet. The oscillations were attributed to a shock induced instability and were successfully eliminated by the use of shock strips.⁶ The location of the shock was computationally predicted through steady simulations by Fuglsang *et al.*⁶ using a Body-Fin-Rudder geometry.

Experimentally there were a number of important studies in the 1960's and 1970's exploring the buzz phenomenon.⁷⁻⁹ The popular classification of buzz in the literature was defined by Lambourne.⁷ During the course of his experiments he found that there are 3 main types of buzz possible which he called Type A, B and C. Type A buzz occurs when the shock stands somewhere ahead of the flap hinge line and interacts with the boundary layer and the flap motion. The limit cycle oscillation is brought about by the synchronisation of the shock strength and motion, the flow separation and the angular flap motion. As the control surface moves it alternately weakens or strengthens the shock, causing separation and reattachment of the flow. The separated flow in turn creates a hinge moment at the flap leading edge which makes the flap undergo oscillation. The Type A buzz is limited to thick aerofoils and is rarely seen in aerofoils with less than 10% camber.¹⁰ Shock induced flow separation is the primary requirement for Type A buzz to occur. Type B buzz is when the shock crosses the hinge line and translates over the control surface. The driving mechanism here is the unsteady hinge moment from the pressure pulse created by the shock motion. The hinge moments involved in Type B buzz are greater than in Type A and are much more difficult to alleviate.

Until now there have been few numerical simulations of buzz described in the literature. One of the first such studies was performed by Steger¹¹ who carried out a 2D buzz simulation on a P-80 wing using an implicit finite difference code capable of solving the RANS equations. The P-80 aircraft was already known to suffer from buzz problems during flight testing and this was further investigated in the NASA Ames wind tunnel by Erickson and Stephenson.¹² Steger was able to match the computed results with the experiments, and also measured the effect of viscosity on buzz simulations. It was found that for a certain Mach number the oscillations in an inviscid calculation would die down after an initial kick but that the oscillations in viscous simulations would result in a limit cycle.¹¹ At a higher Mach number the inviscid simulation would diverge whereas the RANS simulation would still predict a limit cycle. Hence he deduced that viscosity had an effect of both preserving and mitigating the oscillations.

Bendiksen numerically investigated a type of buzz instability that relies purely on the interaction between the shock and flap motion, which he termed non-classical buzz.¹⁰ He showed that for certain cases, especially for thin aerofoil sections, the flow separation does not play an important role in maintaining a limit cycle oscillation. A buzz boundary traced from inviscid calculations compared well with experiments.¹⁰ Recently the non-harmonic motion of the shock over an aerofoil with a harmonically oscillating flap¹³ and 3D aileron buzz calculated using the thin layer RANS equations were shown.¹⁴

The current paper aims to study qualitatively the Goshawk rudder buzz reported in.⁶ The models are based on the BAE SYSTEMS Hawk trainer, of which the Goshawk is a derivative. The purpose of the work reported is to demonstrate the CFD based simulation capability on an example which has several challenging features, namely a moving control surface and shock wave. The simulation challenge of treating moving control surfaces is first considered, followed by consideration of the steady state CFD results, followed by dynamic simulations of buzz.

II. Formulation

A. Fluid and Structural Solver

The Euler and RANS equations are discretised on curvilinear multi-block body conforming grids using a cell-centred finite volume method which converts the partial differential equations into a set of ordinary differential equations. The convective terms are discretised using Osher's¹⁵ upwind method. Monotone Upwind Scheme for Conservation Laws (MUSCL) variable extrapolation (see Van Leer¹⁶) is used to provide second-order accuracy with the Van Albada limiter to prevent spurious oscillations around shock waves. Following Jameson,¹⁷ the spatial residual is modified by adding a second order discretisation of the real time derivative to obtain a modified steady state problem for the flow solution at the next real time step, which is solved through pseudo time. This pseudo time problem is solved using an unfactored implicit method, based on an approximate linearisation of the residual. The linear system is solved in unfactored form using a Krylov subspace method with Block Incomplete Upper Lower (BILU) preconditioning. The preconditioner is decoupled between blocks to allow a very high efficiency on parallel computers with little detriment to the convergence of the linear solver. For the Jacobian matrix of the CFD residual function, approximations are made which reduce the size and improve the conditioning of the linear system without compromising the stability of the time marching.

This formulation is implemented in the flow code Parallel Multiblock (PMB). The equations are solved on block structured grids. A wide variety of unsteady flow problems, including cavity flows, aerospike flows, delta wing aerodynamics, rotorcraft problems and transonic buffet have been studied using this code. More details on the flow solver can be found in Badcock et al.¹⁸

The geometries of interest deform during the motion and the mesh must be moved to conform with the evolving geometry. This is achieved using Transfinite Interpolation (TFI) of displacements within the blocks containing the aircraft. The surface deflections are interpolated to the volume grid points \mathbf{x}_{ijk} as

$$\delta\mathbf{x}_{ijk} = \psi_j^0 \delta\mathbf{x}_{a,ik} \quad (1)$$

where ψ_j^0 are values of a blending function (see Gordon and Hall¹⁹) which varies between one at the aircraft surface and zero at the block face opposite. The surface deflections $\mathbf{x}_{a,ik}$ are obtained from the transformation of the deflections on the structural grid and so ultimately depend on the values of the generalised structural coordinate η_i (defined below). The grid speeds can be obtained by differentiating equation (1) to obtain their explicit dependence on the values of $\dot{\eta}_i$.

Finite element methods allow for the static and dynamic response of a structure to be determined. Stiffness (K) and mass (M) matrices are used to determine the equation of motion of an elastic structure subjected to an external force \mathbf{f}_s as

$$\mathbf{M}\ddot{\delta\mathbf{x}}_s + \mathbf{K}\delta\mathbf{x}_s = \mathbf{f}_s \quad (2)$$

where $\delta\mathbf{x}_s$ is a vector of displacements on a grid of points \mathbf{x}_s . Because the structural system under consideration is assumed to be linear, its characteristics are determined once and for all prior to making the flutter calculations, so that M and K are constant matrices generated, in this case, by the commercial package MSC/NASTRAN.

The aircraft deflections $\delta\mathbf{x}_s$ are defined at a set of grid points \mathbf{x}_s by

$$\delta\mathbf{x}_s = \sum \eta_i \phi_i \quad (3)$$

where ϕ_i are the mode shapes and η_i the generalised displacements. Projecting the finite element equations onto the mode shapes results in the equations

$$\frac{d^2\eta_i}{dt^2} + \omega_i^2 \eta_i = \phi_i^T \mathbf{f}_s \quad (4)$$

where \mathbf{f}_s is the vector of external forces at the structural grid points. This equation can be solved by a two stage Runge-Kutta method, which requires a knowledge of \mathbf{f}_s^n and \mathbf{f}_s^{n+1} .

B. Transformation Between Fluid and Structural Grids

The CVT scheme is a transformation technique proposed in Goura.²⁰ Each fluid surface grid point is first associated with a triangular element on the structural grid. The projection of the fluid point onto the triangle is moved linearly with respect to the structural points. The vector connecting the projected point and the fluid surface point is rotated to keep it normal to the plane of the triangle, and the magnitude is scaled to keep the volume of the tetrahedron formed by the three structural points and the fluid point constant.

C. Example for Civil Configuration

In the aeroelastic analysis of a complete aircraft the deforming components need to be blended together to maintain the grid fidelity at the component interfaces. This is especially true if the two components are undergoing large deformation in different planes resulting in large gaps at the interfaces. This can happen at the wing-fuselage interface when the FEM model is inadequately constrained at the wing root and hence the wing root does not follow the fuselage properly. According to the dependence of the deformation of a given component to the deformation of other components it can be classified into a hierarchy.²

The deformation of a lower hierarchy component is influenced by the deformation of the higher hierarchy component. The strength of this influence is calculated from weights and depends on the distance of a node on the lower hierarchy component from the nearest node on the upper level component. Melville suggested that typically the fuselage occupies the first level of the hierarchy as all other components are attached to it.² The wings, fin and the tailplane occupy the second level and the missiles, control surface, pylons etc the third level. The strength of the influence of the higher hierarchy component on the lower hierarchy component can be controlled by the blending parameter used. A multi-level blending scheme for aeroelastic simulation for complete aircraft configuration was proposed in²¹ and subsequently applied on the Hawk wing body aeroelastic case.²⁶ The general method of calculating the deformation of a fluid surface node $\mathbf{x}_{a,l}$ on a multilevel configuration is,

$$\delta \mathbf{x}_{a,l} = \sum_{m=1}^n w_{m,l} \delta \mathbf{x}_a^m. \quad (5)$$

The subscripts a, l denote the l^{th} node of the aerodynamic surface grid a . The superscript m is the level to which the node or the deformation belongs and $w_{m,l}$ is the weighting factor which determines the contribution to the total deformation of the surface node due to its own deformation and the deformation of the nearest higher hierarchy node. The weights depend on the distance between the surface node and nearest higher hierarchy node $d_{m,l}$ and are calculated as follows,

$$w_{1,l} = e^{-10d_{m,l}} \quad (6)$$

and

$$w_{2,l} = 1 - w_{1,l}. \quad (7)$$

Figure 1 shows $w_{1,l}$ of the structure calculated over the aircraft for 2 level blending. The exponential blending function e^{-10d} is used in equations 6 and 7 but it can be changed to suit individual test cases. If the blending constant -10 is reduced to lower values the influence of the higher hierarchy component dies off quickly and the width of the green band seen in Figure 1 gets narrower.

The mapping of the aerodynamic grid to the structural grid is one of the central steps in the aeroelastic calculations. In the current work the mapping is done as a preprocessing step before performing the coupled calculations. Figure 2 shows the various components that are assembled for the calculation. The mapping block in the figure involves the identification of the triangular element to which each surface aerodynamic point is anchored, and the calculation of the distance of each point on the lower hierarchy fluid component from the nearest point on an upper hierarchy. This is written down in a mapping file which is used for the CVT and component blending scheme as described in.²¹ Once the mapping file is obtained, the transformation needs to be visually inspected for each mode of the structure. This can be done by forcing the structure to statically deform in each mode without actually performing the fluid calculations. These calculations do not have any physical meaning except for mimicking the surface grid transformation of the individual mode shapes during the actual calculations. The mapping step of Figure 2 is implemented on the Generic Large Aircraft test case in the next section.

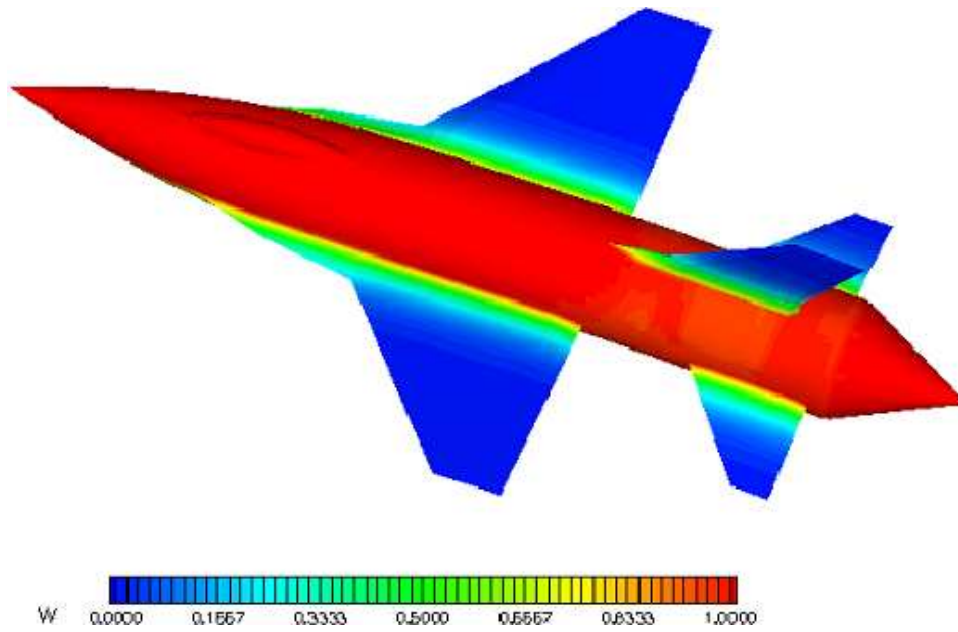


Figure 1. Weighing contours of 2-level mapping on a multi-component test case.

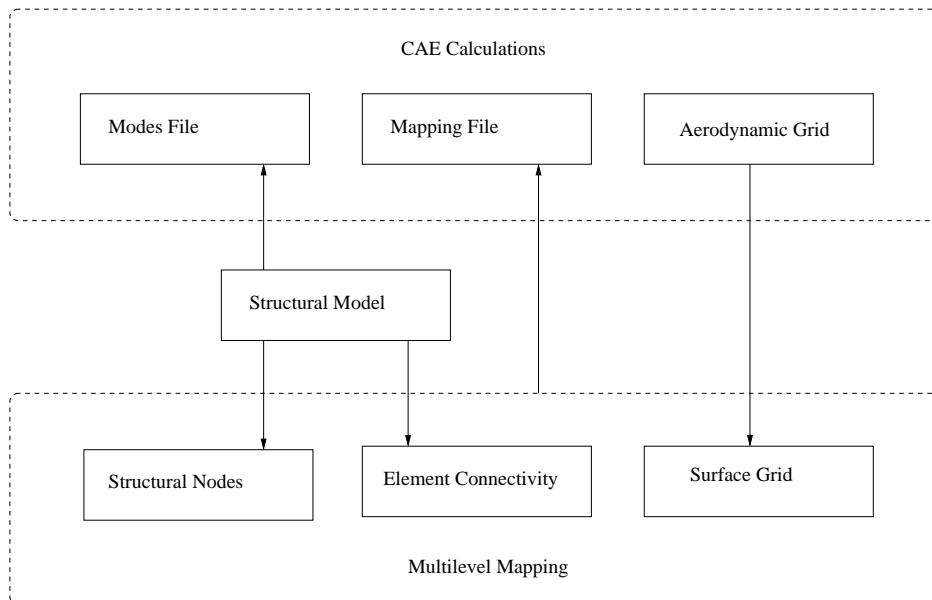


Figure 2. Components of an aeroelastic calculations

D. Transformation of the Generic Large Aircraft

The Generic Large Aircraft (GLA) test case has been adapted from the AIAA Drag Prediction Workshop. It is a relatively complex geometry for nonlinear aeroelastic calculations as there are 3 levels of hierarchy. The first level is the fuselage to which the wing is attached. Here the deformation of the wing root depends on the fuselage, hence it is classified into a second hierarchy component. The pylon is attached to the wing, and at the wing-eylon junction the deformation is due to the wing and hence the pylon is classified as a third hierarchy component. The engine nacelle however is classified into a second level component since the deflection at the junction between the nacelle and the pylon is due to the nacelle and not the pylon. Moreover as the engine is at a distance from the fuselage the influence of the fuselage on the nacelle is negligible on account of the exponential blending parameter used here. Figure 3 shows the hierarchical classification of the structural components of the aircraft. The process for structural classification has the following steps

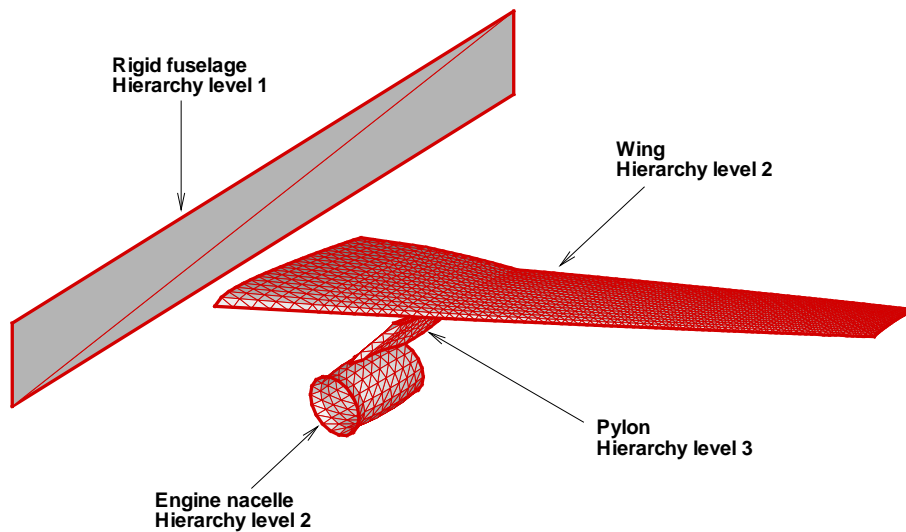


Figure 3. Division of components into hierarchical levels

- The structural nodes for each component are extracted from the FEM grid.
- The extracted grid points are then triangulated using a Delaunay triangulation. The output from this is connectivity data in a file with each element consisting of the line numbers of the 3 nodes from the nodal file. A component label is given to each triangular element, in the current case, 1 for fuselage elements, 0 for wing, 2 for pylon and the 3 for the nacelle.
- The nodal files and the corresponding labelled element connectivity files are assembled into a single node file and a single connectivity file.

As for the elements of the structural components, the nodes lying on the surface of the aerodynamic grid of the various components are also labelled. However the labelling is done during the grid generation step itself. The nodes on the fuselage of the aerodynamic grid are labelled as 50001, on the wing 50000, on the pylon 50002 and on the nacelle

50003. An aerodynamic surface grid file contains the nodal coordinates along with the labels. The linking of the elements of the structural components to the nodes of the corresponding components on the aerodynamic grid is done in a small file. This file classifies the components into their respective hierarchies. For the current case the linking is as follows

```
4
1 50001 1
0 50000 2
2 50002 3
3 50003 2
```

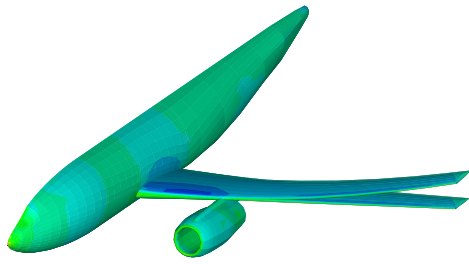
The first line indicates the number of components the geometry contains. The first column specifies the structural component label, the second column specifies the corresponding aerodynamic component it is linked to and finally the third column specifies the hierarchy level of the component. The linking file along with the labelled structural elements file and the labelled aerodynamic surface grid is used for the mapping. For each aerodynamic surface grid point the mapping utility searches for the nearest structural element of the fuselage in the level 1 mapping. In the second level it searches for the nearest fuselage element for the aerodynamic grid points on the fuselage and for the rest of the components it searches for the nearest second hierarchy component structural elements. Finally in the third level the utility searches for the nearest structural element of each component from the aerodynamic point on that corresponding component. This information is written down in the mapping file to be used by the transformation scheme during the coupled calculations. However before the mapping file is used the mapping is inspected by forcing the aerodynamic surface grid to deform in each structural mode to be used in the calculation. The transformed mode shaped of the first 6 modes of the GLA are shown in Figure 4. From visual inspection in the plotting tool TECPLOT these were found to be smooth and maintained the grid quality at component interfaces.

E. Control Surfaces

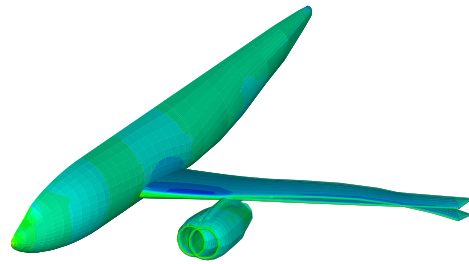
The wing trailing edge control surfaces are usually modelled structurally as plates hinged at its leading edge. The inboard and outboard edges of the control surfaces are free and not blended with the wing. Computational simulations involving moving control surfaces are still not common mainly due to the difficulty in treating the grid over and around the control surfaces. The free edges of the flap cause a geometrical discontinuity along the wing span which is difficult to treat within the framework of a multiblock code. One of the simplest techniques is the blending of inboard and outboard edges of the flap with the wing surface. The blending does cause a deviation from the proper representation of the flap geometry and the effect the blending has on the flow solution needs to be assessed. Another option for modelling the flap is the introduction of small gaps between the inboard/outboard flap edges and the wing. When the flap is deflected along its hinge the cells in these gap blocks are sheared as shown in Figure 5. A flap modelled in this way maintains its geometric details but there is a penalty to be paid in computational time as the grid quality inside the sheared gap blocks is poor. When blended control surfaces are used in the aeroelastic simulation the blending is easily implemented in the calculation while maintaining a reasonable grid quality, even for very large flap deflection angles. The blending of inboard and outboard flap edges is carried out here using a three level hierarchical blending scheme. For the flap this means that the inboard and outboard edges are driven by the wing and the flap nodes adjacent to the edge nodes are driven by a combination of wing and flap deformations. The extent of the influence of the fin/fuselage on the flap depends on the blending parameter hence the choice of the blending parameter controls the extent of blended length of the flap. The choice of the blending parameter depends on the extent of mismatch at the component interface. A very large mismatch will require a smaller absolute value of the blending parameter which means a large area of the lower hierarchy component will be influenced by the higher hierarchy component. A larger value will limit this influence to a smaller area of the lower hierarchy component

F. Summary of Results for SST configuration

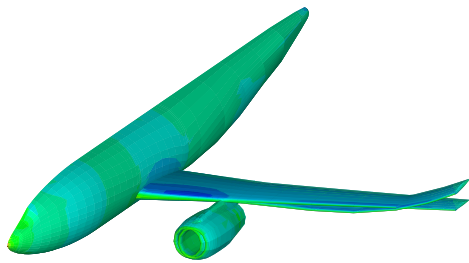
The SST arrow wing²² is a cranked double delta with a root chord of 2.103 metres. A half model is used in the experiments with a semi-span of 1 metre. The section profile is



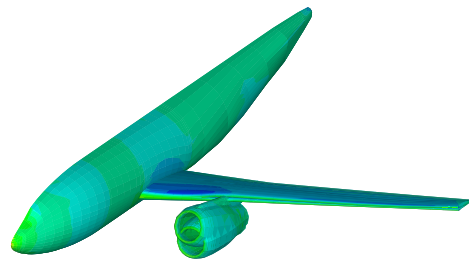
(a) Mode 1 0.56 Hz



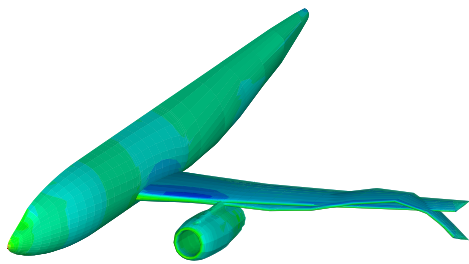
(b) Mode 2 1.65 Hz



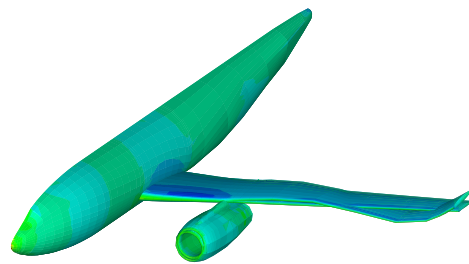
(c) Mode 3 1.93 Hz



(d) Mode 4 2.69 Hz



(e) Mode 5 3.63 Hz



(f) Mode 6 4.23 Hz

Figure 4. Transformed mode shapes of the GLA.

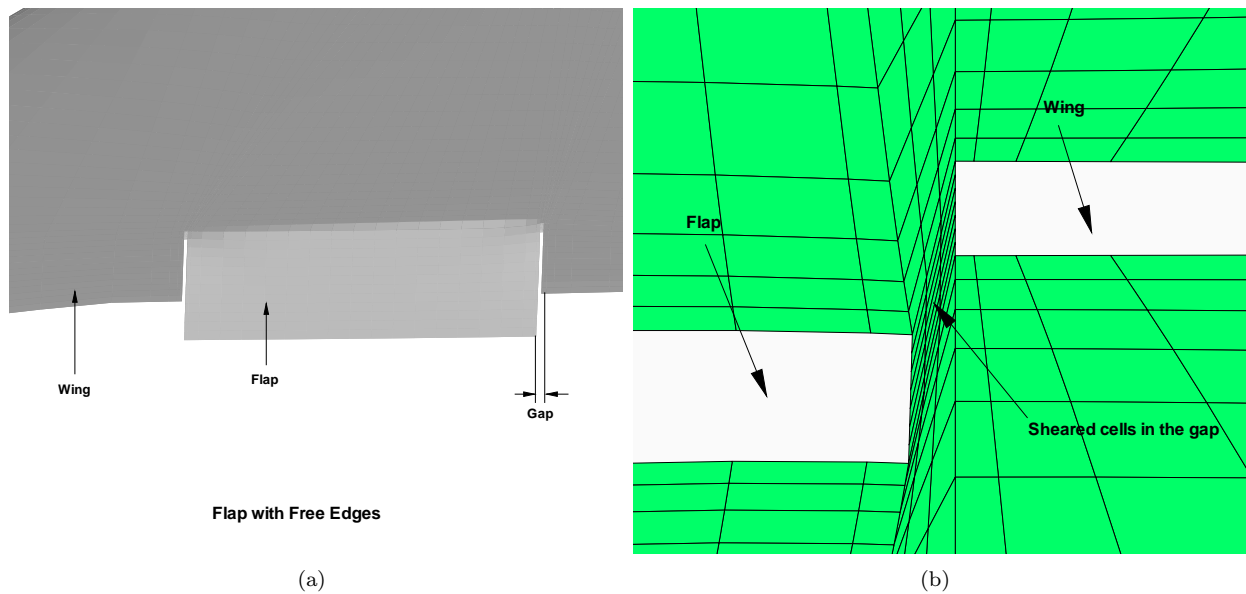


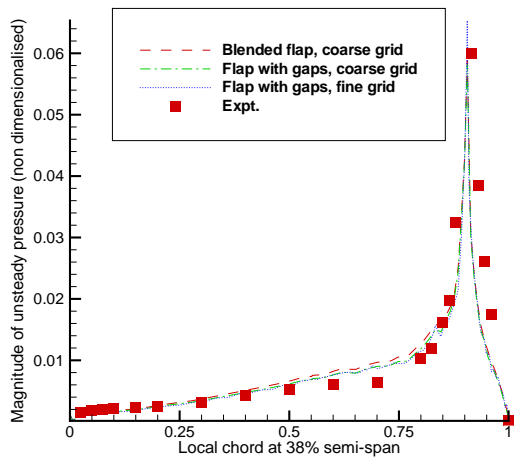
Figure 5. A deployed trailing edge flap with free edges

a NACA 0003. The inboard delta has a sweep angle of 72.8° and the outboard a sweep of 51.6° . The trailing edge flap starts at 20% half-span and terminates at 50% half-span. The flap chord is 0.11 metres. Experimental data is available for a range of Mach numbers between 0.79 and 0.91, angles of attack of 0° , -2° and -4° , flap mean angles of 0° , -5° and 5° and FOFs of 5 Hz, 10 Hz, 15 Hz, 20 Hz, 25 Hz and 30 Hz.

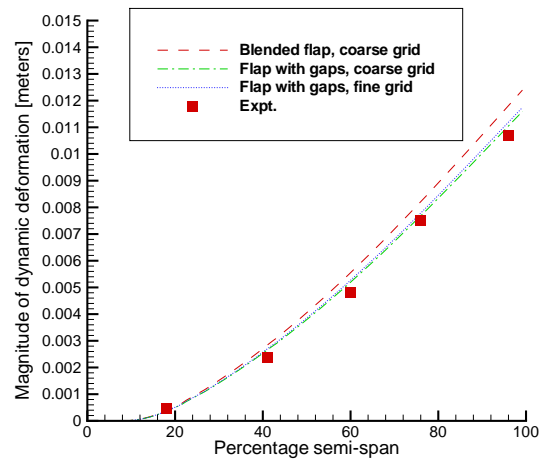
Along with the measured unsteady pressure and deformation, FEM data in the form of a structural grid and computed natural modes of vibration are also provided in the paper.²² A brief description of the structure of the experimental model is presented in an earlier paper by Tamayama.²³ The wing structure is made up of a 7 mm thick aluminium plate with holes drilled to make it flexible. It was found in the experiments that the frequency of the first wing bending mode increased from 9.79 Hz in vacuum to around 15 Hz at Mach 0.8.²³ As the frequency of this mode lies in the vicinity of the forced FOFs (5 Hz-30 Hz) and as the frequency of the next natural mode is higher (40.25 Hz) almost all the deformation of the structure is contributed by the first wing bending mode.

Computations have been done for this case for forced flap motions²⁴ and buzz.²⁵ To assess the effect of the blended edges on the computed unsteady pressure and deformation an inviscid simulation was performed using flaps with free edges. Figure 6 compares the unsteady pressure and deformation for a forced motion of 15 Hz obtained from a blended flap and the flap with free edges. There is little difference seen in the computed results although the blended flap predicts a slightly bigger dynamic deformation on account of it having a larger flap surface area. A full discussion of these results can be found in reference.²⁴

Next the influence of the flap treatment on a buzz response is calculated. The buzz is driven by a shock moving onto the control surface. In the first case a low blending parameter of 20 and in the second a higher blending parameter of 100 is used. The larger the value of the blending parameter the more the transformed fluid grid conforms to the structural grid at the given transformed mode. For the flap mode where the flap nodes move relative to the wing nodes the blending parameter acts as a damper limiting the motion of the flap. This damping effect decreases with the increasing value of the blending parameter. Also a higher blending parameter maintains the proper shape of the flap as shown in Figure 7. The choice of the parameter depends on the dimensions of the flap and shape of the mode. Figure 8 shows the angle against time for the two values of blending parameter. The flap modelled with a blending parameter of 20 has, in general, a more restrained response both in amplitude and in frequency.



(a) Unsteady pressure at 38% semi-span location.



(b) Unsteady deformation along the span.

Figure 6. Unsteady pressure and deformation plots for the SST forced flap computations on a coarse and fine grids using flaps with gaps and at FOF of 15 Hz using the Euler equations. The case conditions are $\alpha = 2^\circ$, $M_\infty = 0.8$, flap rotation amplitude 1.448° .

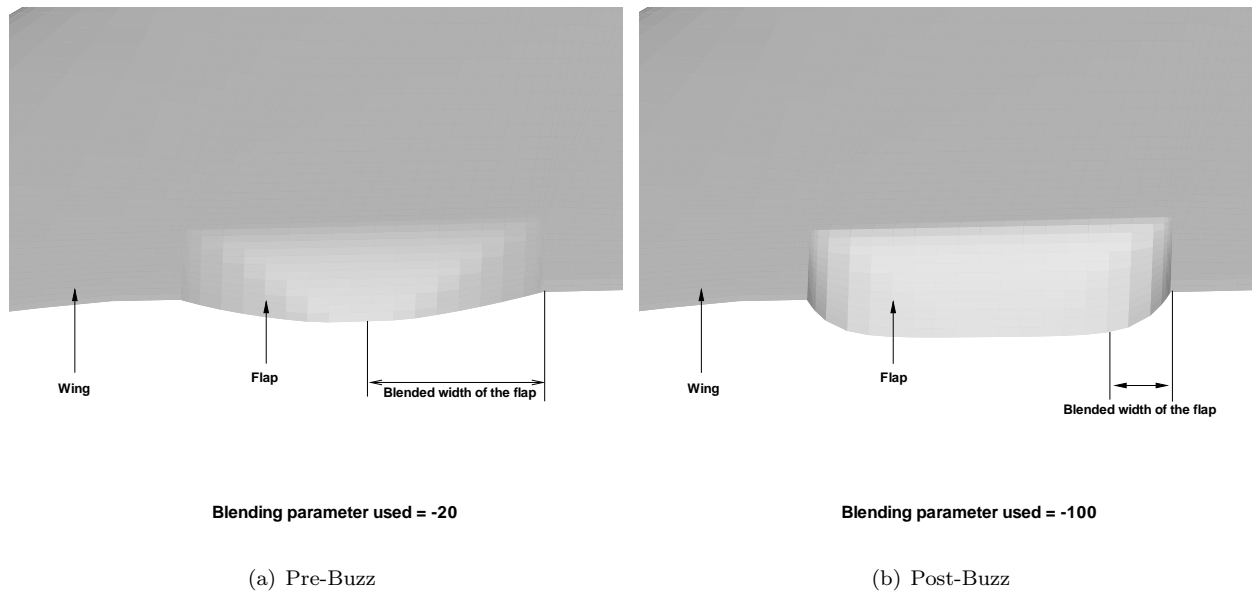


Figure 7. Transformed flap mode using two different values of blending parameter

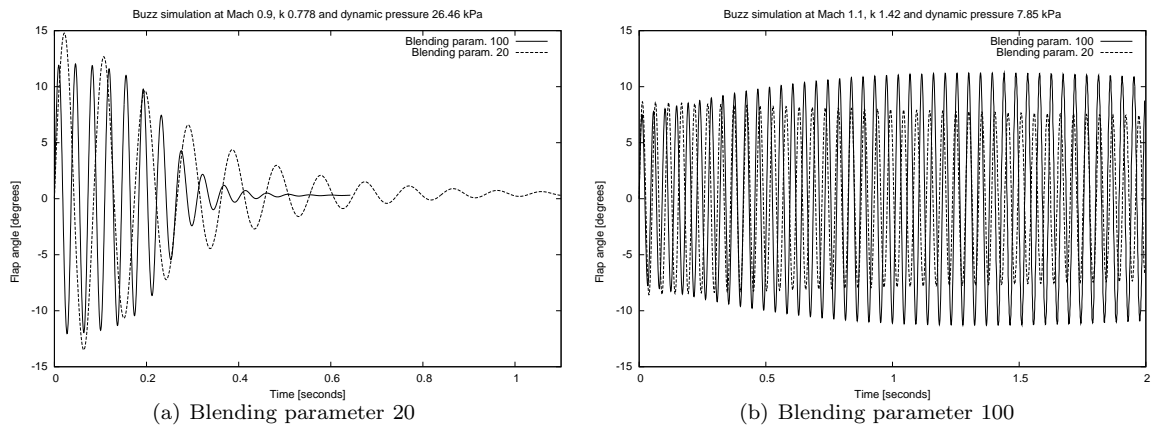


Figure 8. Flap response at different values of blending parameter

III. Fighter Trainer Model

A. Models and CFD Grids

1. Overview and Scope

Fuglsang⁶ reported on rudder oscillations for the T-45A Goshawk which arose at Mach 0.95 and 20,000 feet altitude during a development flight test program. A study based on the geometry and structural behaviour of the BAE SYSTEMS Hawk aircraft was undertaken to demonstrate the feasibility of simulating rudder buzz in the time domain. The geometry has been simplified so that it doesn't include features mounted on the fin (for example the radar receiver) and the structural model is also simplified as described below. The resulting case is thought to retain features representative of the Goshawk incidents but is not a quantitative simulation of the behaviour of the Hawk or Goshawk.

2. Body-Fin-Rudder Case

The oscillations on the Goshawk were assumed to be shock induced and a steady state CFD analysis was performed on the Body-Fin-Rudder (B-F-R) configuration to locate the position of the assumed shock. A strong shock was predicted at Mach 0.95 just ahead of the rudder hinge on the B-F-R configuration using a RANS based CFD code TLSN3D. The instability observed in the flight test at Mach 0.95 was attributed to this. In the current work a similar B-F-R configuration is analysed. A grid was constructed with 540,000 points and a wall spacing of $10^{-3}c$. The blocking consists of an O-type block over the fuselage and an H-type over the fin and rudder as shown in Figure 9. There are 9500 points on the surface of the aircraft.

3. Body-Fin-Rudder-Tail Case

Analysing the results of the B-F-R case it was felt that a more detailed representation of the aircraft may be required in order to get realistic aerodynamic results over the fin and the rudder. This is important as an interaction between the fin-rudder structure and the oscillating shock is observed in the unsteady simulation. To improve on the flow predicted over the fin the interference effects from the adjacent aircraft components may need to be included. Hence the tailplane was added to the simulated geometry. It was found that viscous effects were minimal over the fin and did not alter the predicted location of the shock significantly for the Body-Fin-Rudder case and hence only the inviscid calculations are performed for the rest of the cases. The Body-Fin-Rudder-Tail (B-F-R-T) case has an C-H blocking over the fin-rudder and an O-block over the tail and the fuselage (see Figure 10). The wall spacing is $10^{-3}c$ and the size of the coarse and fine grids are 300 thousand and 2 million points respectively.

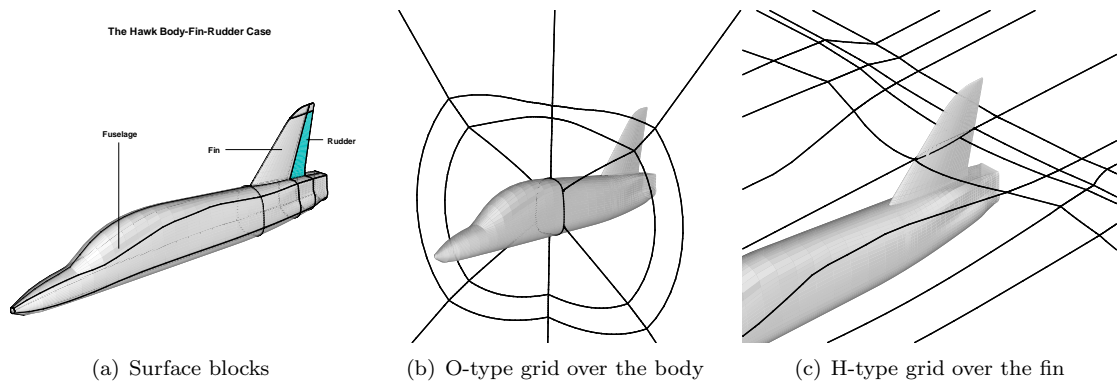


Figure 9. The blocking topology of the Hawk Body-Fin-Rudder test case

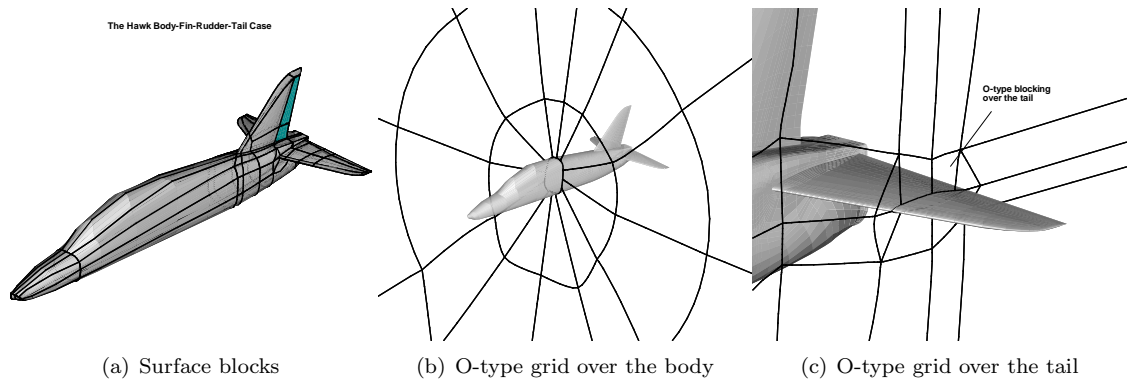


Figure 10. The blocking topology of the Hawk Body-Fin-Rudder-Tail test case

4. Body-Fin-Wing-Rudder-Tail Case

When the tail was included in the simulation the steady pressure distribution changed to a very large extent. This gave an indication that at transonic Mach numbers the interference of other components has a very big impact on the pressure distribution. Recognising this the wing was also included in the simulation to model the component interference. It should be noted that the engine bulge on the fuselage and the radar on the fin have been not included in this simulation. The blocking is an extension of the B-F-R-T grid and consists of an O-block over the fuselage, the tail and the wing whereas the fin-rudder has a C-H blocking. The size of the grids are 310 thousand and 2.1 million points for coarse and fine levels respectively.

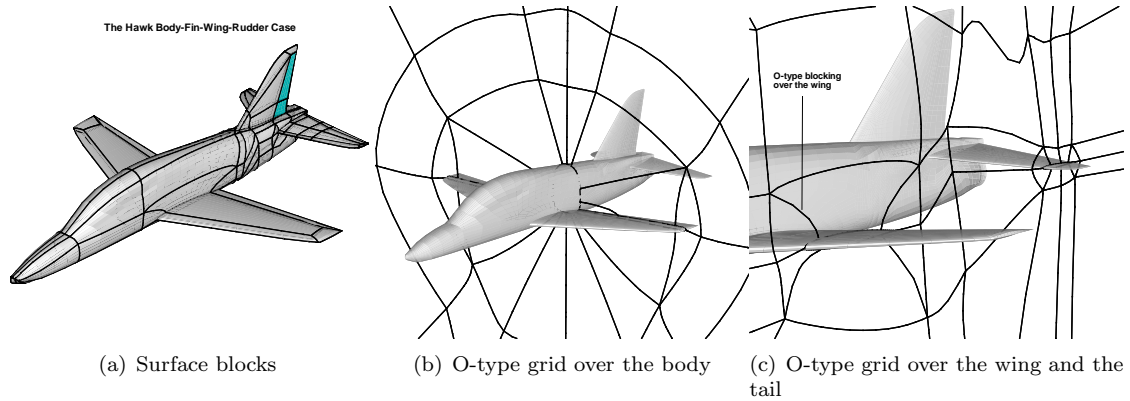


Figure 11. The blocking topology of the Hawk Body-Fin-Wing-Rudder-Tail test case

B. Structural Model and Transformation

The structural model is derived from a version of the Hawk Nastran aeroelastic analysis deck used at BAE SYSTEMS. The structural half model is a lumped mass model with 1D bar elements to model the aircraft components. For our purpose all the nodes except those modelling the fin and rudder are constrained in all of the six degrees of freedom. Hence the whole aircraft except the fin and rudder is kept rigid. Modal analysis is performed and the first 4 natural modes of vibration of the fin-rudder are extracted from the Nastran output file and converted into the format required by the flow solver using a parser utility. The structural nodes required for the representation of the aircraft are extracted from the Nastran output file and labelled for the multi-level transformation using an extraction utility. The extracted structural nodes are triangulated using an open source software TRIANGLE. The first four natural modes are used in the analysis. Table 1 gives the natural frequency of these modes. One of the important issues in a CFD based aeroelastic analysis is the transformation between the structural and the fluid grids. Before commencing the unsteady calculations the transformation is checked by visually inspecting the statically deformed modes. Figure 12 shows the forced modal deformation on the structural grid and the corresponding transformed modes on the fluid grid of the B-T-F-R case.

	Frequency (Hz)	Description
Mode 1	18.8	Rudder Rotation
Mode 2	22.3	First fin bending
Mode 3	62.2	First fin torsion
Mode 4	71.3	Second wing bending

Table 1. Natural frequencies and mode description of the Hawk fin-rudder structural model.

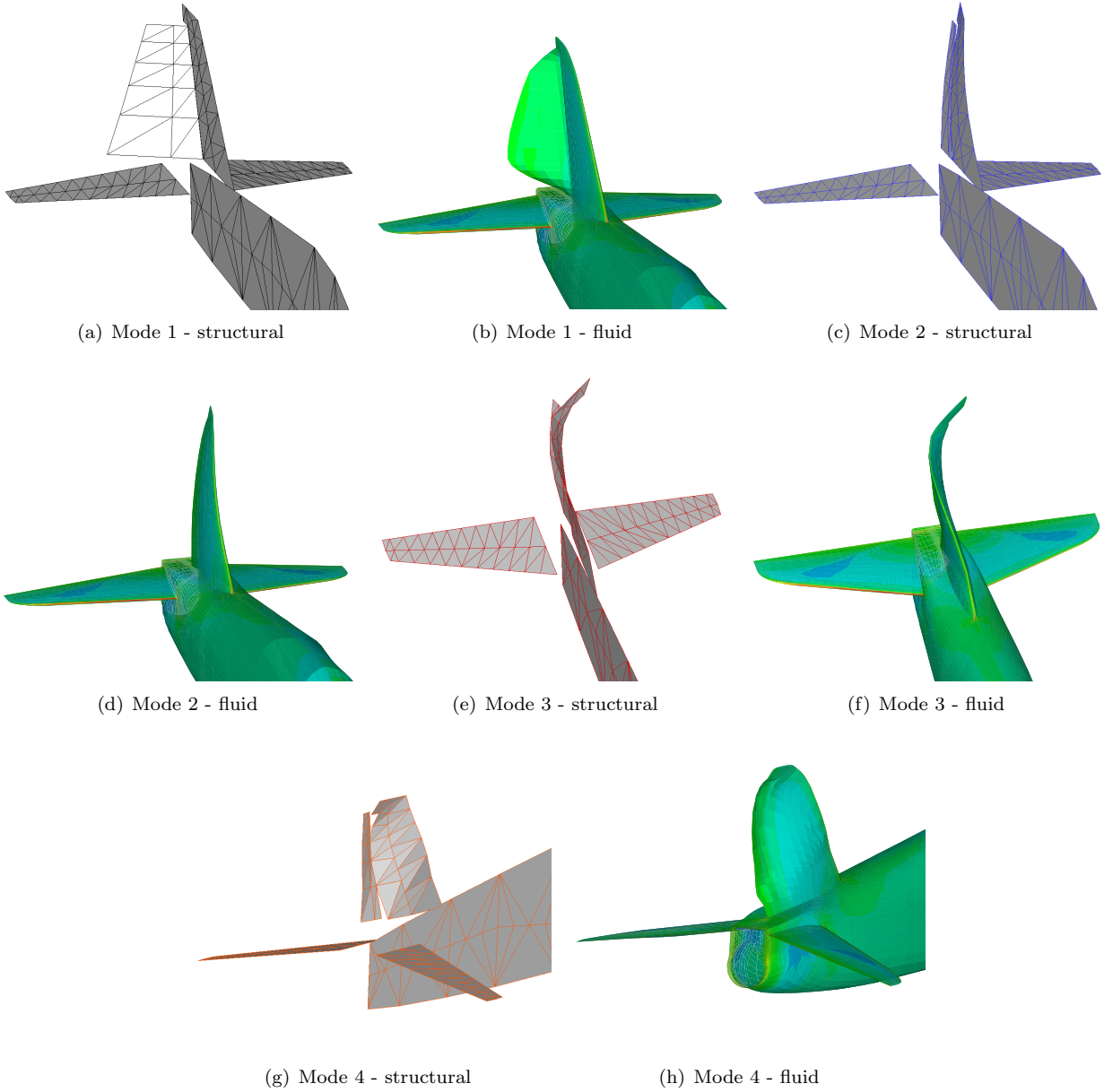


Figure 12. The structural mode shapes are transformed on to the fluid surface grid to visually verify the accuracy of the transformation. A medium fluid grid of the Hawk B-F-R-T case is used for the visualisation.

IV. Rudder Buzz

A. Steady Results

Surface pressure cuts were made on the fin at five horizontal locations shown in Figure 13. The C_p values are compared for three cases of increasing geometric complexity B-F-R, B-F-R-T and the B-F-W-R-T cases. Results from an Euler simulation provided by BAE SYSTEMS for a detailed geometry simulation, including all aircraft components and the radar receiver on the fin are included in the comparisons. In Figures 14 to 18 it can be seen that the B-F-W-R-T case compares closest to the BAE SYSTEMS result mainly due to the fact that the wings defuse the shock over the fin. The B-F-R case is seen to predict a strong shock on the rudder hinge. This can cause the corresponding unsteady simulation to predict a shock induced instability which would not be realistic as the shock only exists due to inadequate modelling of the geometry. Another interesting feature of the comparisons is the hump that can be seen between 10 and 10.2 metres on the X-axis and between 2.2 and 2.4 metres semispan in Figures 16 and 17. The radar is not modelled in the current work though it would be expected to influence the pressure distribution over the fin. From these results it is also seen that the full F-B-W-R-T case comes closest to the completely modelled geometry and predicts a relatively strong shock which can induce the control surface instability.

The computational work done on the T45 aircraft by Fuglsang *et al.*⁶ to investigate the rudder buzz incident in the flight test used a simplified configuration of the aircraft ignoring all the components except the body, fin, and rudder. Figure 19 shows the surface pressure plots taken from reference⁶ at 41% and 68% semispan at Mach 0.95. These plots clearly predict the presence of a strong shock near the rudder hinge. A similar calculation was performed on the current B-F-R configuration which also predicts a strong shock near the rudder hinge. However we know from the surface pressure comparison with the full model that this shock will not actually exist on the real aircraft due to the interference effects. An engineering solution to address the rudder buzz was based on the steady calculations performed on this simplified geometry and included the placement of shock strips before the rudder hinge. Shock strips are raised surfaces or "humps" that are used to accelerate the flow and cause a premature shock ahead of the location where a shock would normally occur. Finally Figures 20 and 21 show the surface pressure contours on a cross-sectional plane through the fin at Mach 1.05 for the B-F-R, the B-F-R-T and the B-F-W-R-T cases. A strong shock before the fin can be seen on the cross-sectional plane for the B-F-W-R-T case.

B. Dynamic Results

Dynamic calculations are made to consider the stability of the configuration. Previous work reported in⁵ compared linear and CFD results for the flexible Hawk wing and wing-fuselage-tailplane configurations. Close agreement was obtained in subsonic freestreams. In the current case the only flexibility left in the model is on the fin. In the subsonic region CFD predicts a lower flutter velocity than linear methods. This is likely to be because in the CFD analysis the flow accelerates over the wings and when it finally reaches the fin it is at a higher velocity than the freestream velocity. Interference effects are not included in the linear results.

The effect of component interference on buzz was investigated by performing dynamic analysis on the B-F-R, B-F-R-T and B-F-W-R-T cases. As seen in the steady flow simulations the interference effect of the components has a major effect on the shock strength on the fin and hence the pressure distribution. The pressure distribution on the B-F-W-R-T at 2.2 metres span for various Mach numbers is shown in figure 22. It can be seen that the shock is absent on the rudder at low transonic Mach numbers. At higher Mach numbers the shock reforms on the fin. As the Mach number increases further the shock on the fin weakens again. Matched point analysis was performed at 10,000 feet and at Mach 0.97 on the three cases to investigate the presence of the buzz instability. Figure 23 shows the modal response of the rudder rotation mode. It is seen that for the complete B-F-W-R-T case the initial perturbation damps down in time. In Figures 20 and 21 the B-F-W-R-T case in comparison to the other two cases has the weakest shock. The B-F-R and the B-F-R-T cases do undergo buzz at Mach 0.97 due to the presence of the shock. It is seen that the amplitude of oscillation is greater for the B-F-R-T case as the presence of a tail

changes the shock location to the rudder trailing edge. These results tend to confirm the conclusions drawn from the steady shock locations. The results show that type B buzz (driven by shock motion rather than separation) might not have been the cause of the Goshawk rudder buzz described in the literature, and is not a concern for the Hawk, as confirmed in flight. The simplified B-F-R and B-F-R-T results are misleading in that they show that the type B buzz is present, but this is a result of geometrical simplifications causing erroneous shock positions and strengths.

V. Conclusions

The simplified treatment of control surfaces was considered and a method of blending into the wing or fin component evaluated. A case study of the transformation between fluid and structural grids was shown for a commercial aircraft configuration featuring a nacelle.

A systematic study of rudder buzz on a fighter aircraft was then made. Steady state solutions were examined for various geometric configurations to identify shock locations. It was concluded that the interference between components is significant. Time domain simulations of rudder buzz were then achieved. These confirmed that type B buzz is not present for the generic Hawk configuration studied, as confirmed by in-flight behaviour. The geometrical simplifications used in previous studies lead to errors in the shock strength and location, which lead to spurious instances of type B buzz.

The current work suggests that this sort of dynamic behaviour can be simulated should such a situation arise during aircraft development or operation.

Future work will focus on reduced order modelling of buzz phenomena. Methods have been developed to calculate, for example, the onset Mach number of an aeroelastic instability²⁶ and work is ongoing to generate a reduced (two degree of freedom) model to calculate the LCO response. This method will be exercised on the case considered in this paper, to allow high fidelity simulation of buzz at a cost comparable to steady state cost.

VI. Acknowledgements

This work was supported by BAE SYSTEMS, Engineering and Physical Sciences Research Council and Ministry of Defence, and is part of the work programme of the Partnership for Unsteady Methods in Aerodynamics (PUMA) Defence and Aerospace Research Partnership (DARP).

References

- ¹Dreim, D.R., Jacobsen, S.B. and Britt, R.T., Simulation of non-linear transonic aeroelastic behaviour on the B2. in Proceedings of International Forum on Aeroelasticity and Structural Dynamics, 1999, NASA/CP-1999-209136, 1999.
- ²Melville, R., Nonlinear Simulation of F-16 Aeroelastic Instability, AIAA Paper 2001-0570, January, 2001.
- ³Pranata, B.B., Kok, J.C., Spekrijse, S.P., Hounjet, M.H.L and Meijer, J.J. Simulation of limit cycle oscillation of fighter aircraft at moderate angle of attack. in the Proceedings of International Forum on Aeroelasticity and Structural Dynamics, CEAS/AIAA, Amsterdam, June, 2003.
- ⁴Morton, S.A. and Cummings, R.M., Computing Unsteady Loads of Fighter Aircraft at High Angles of Attack and in Maneuvering Flight, NATO RTO AVT-123 RSY-019, Budapest, April, 2005.
- ⁵Woodgate, M.A, Badcock, K.J., Rampurawala, A.M., Richards, B.E., Nardini, D and Henshaw, M.J., Aeroelastic Calculations for the Hawk Aircraft Using the Euler Equations, J Aircraft, 40(4), 2005, 1005-1012.
- ⁶Fuglsang, D.F., Brase, L.O. and Agarwal, S. A Numerical Study of Control Surface Buzz Using Computational Fluid Dynamics Methods, 10th AIAA Applied Aerodynamics Conference, AIAA Paper 92-2654, June, 1992.
- ⁷N. C. Lambourne. Control surface buzz. *Aircraft Research Council R & M*, No. 3364, 1964.
- ⁸Y. Nakamura. Some contributions on a control surface buzz at high subsonic speeds. *Journal of Aircraft*, Vol.5(2):pp. 118, 1968.
- ⁹Y. Nakamura and L. Woodgate. Effects of Reynolds number and frequency parameter on control surface buzz at high subsonic speeds. *Aeronautical Research Council R & M*, No. 3702, 1972.
- ¹⁰O. O. Bendiksen. Nonclassical aileron buzz in transonic flow. *34th AIAA/ASME/ASCE/AHS/ASC Structures, Structural Dynamics and Materials Conference*, (AIAA Paper 93-1479), April 1993.
- ¹¹J. L. Steger and H. E. Bailey. Calculation of transonic aileron buzz. *AIAA Journal*, Vol.18(3):pp. 249-255, 1980.

- ¹²A. L. Erickson and J. D. Stephenson. A suggested method for analyzing for transonic flutter of control surfaces based on available data. *NACA RM A7F30*, 1947.
- ¹³T. A. Weisshaar M. Tamayama and J. Nakamichi. Unsteady shock wave motions on a thin airfoil at transonic speeds caused by an aileron oscillation. *International Forum on Aeroelasticity and Structural Dynamics - Amsterdam*, June 4–6 2003.
- ¹⁴G. Yang and S. Obayashi. Aileron buzz simulation using an implicit multiblock aeroelastic solver. *Journal of Aircraft*, Vol.40(3):pp. 580–589, 2003.
- ¹⁵Osher, S. and Chakravarthy, S. Upwind Schemes and Boundary Conditions with Applications to Euler Equations in General Geometries. *Journal of Computational Physics*, Vol. 50, pp 447-481, 1983.
- ¹⁶Van Leer, B. Towards the Ultimate Conservative Conservative Difference Scheme II: Monotonicity and Conservation Combined in a Second Order Scheme. *Journal Computational Physics*, Vol 14, 361-374, 1974.
- ¹⁷Jameson, A. Time dependent calculations using multigrid, with applications to unsteady flows past airfoils and wings. *AIAA Paper 91-1596*, 1991
- ¹⁸Badcock, K.J., Richards, B.E. and Woodgate, M.A. Elements of Computational Fluid Dynamics on Block Structured Grids using Implicit Solvers. *Progress in Aerospace Sciences*, vol 36, 2000, pp 351-392.
- ¹⁹Gordon, W.J. and Hall, C.A. Construction of curvilinear coordinate systems amd applications to mesh generation. *Int J Num Meth Engr*, 7, 1973, pp 461-477.
- ²⁰Goura, G.S.L, Time marching analysis of flutter using Computational Fluid Dynamics, PhD thesis, University of Glasgow, 2001.
- ²¹Rampurawala, A.M., An assessment of inter-grid transformation for a whole aircraft, MSc Thesis, University of Glasgow, 2002.
- ²²Tamayama, M., Saitoh, K., Matsushita, H. and Nakamichi, J. NAL Arrow Wing with Oscillating Flap, Verification and Validation Data for Computational Unsteady Aerodynamics, RTO Technical Report–26, October, 2000, 295–318.
- ²³Tamayama, M. and Nakamichi, J. Unsteady Aerodynamics Measurements on an Elastic Wing Model of SST, *AIAA Paper 97-0836*, 1997.
- ²⁴Rampurawala, A.M. and Badcock, K.J., Treatment of Forced Flap Motions for Aeroelastic Simulations of an Arrow Wing. *AIAA Paper 2005-4962*, *AIAA Applied Aerodynamics Conference*, Toronto, 2005.
- ²⁵Rampurawala, A.M. and Badcock, K.J., Buzz Simulation for a supersonic transport configuration, *International Forum on Aeroelasticity and Structural Dynamics*, Munich, June, 2005, Paper IF-005.
- ²⁶Badcock, K.J., Woodgate, M.A. and Richards, B.E., Direct Aeroelastic Bifurcation Analysis of a Symmetric Wing Based on the Euler Equations, *Journal of Aircraft*, 42(3),731-737, 2005.

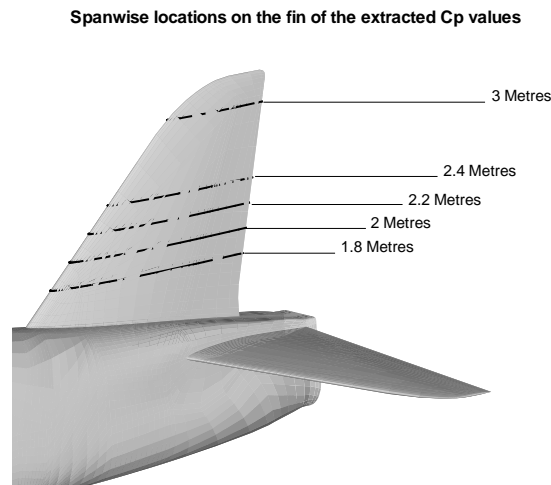


Figure 13. The spanwise locations on the Hawk fin where the Cp values have been extracted for comparison.

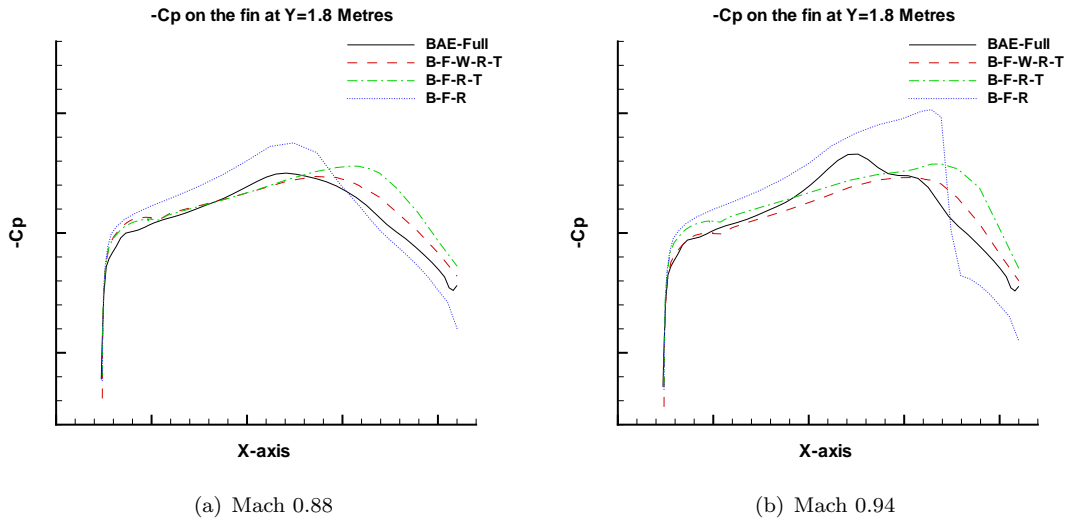


Figure 14. Surface pressure plots on the fin of the complete Hawk configuration at 1.8 Metres span

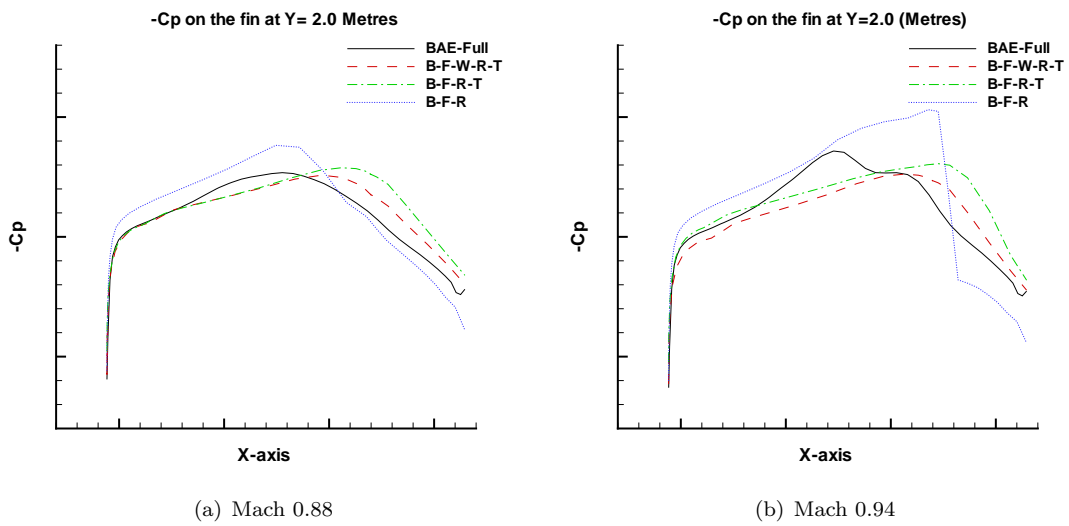


Figure 15. Surface pressure plots on the fin of the complete Hawk configuration at 2 Metres span

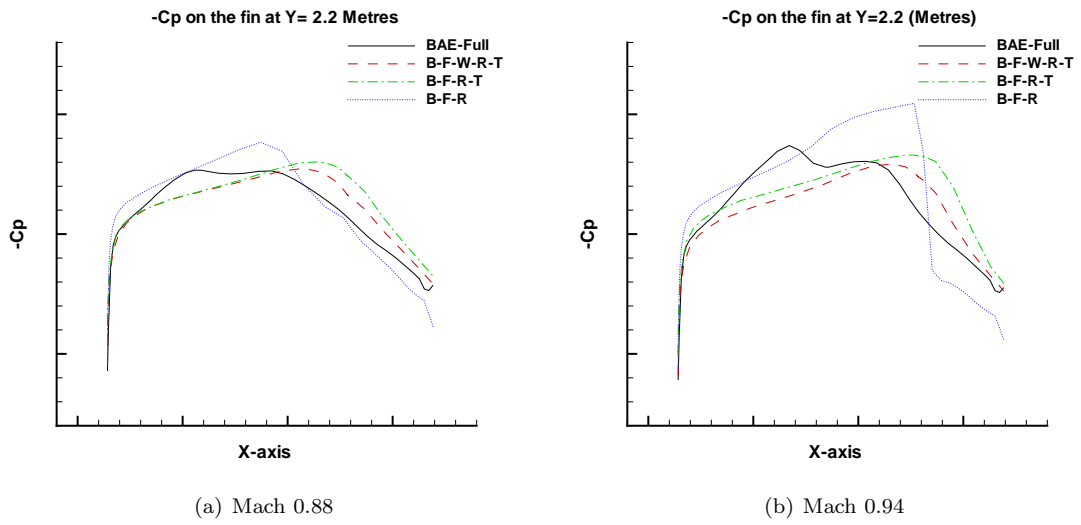


Figure 16. Surface pressure plots on the fin of the complete Hawk configuration at 2.2 Metres span

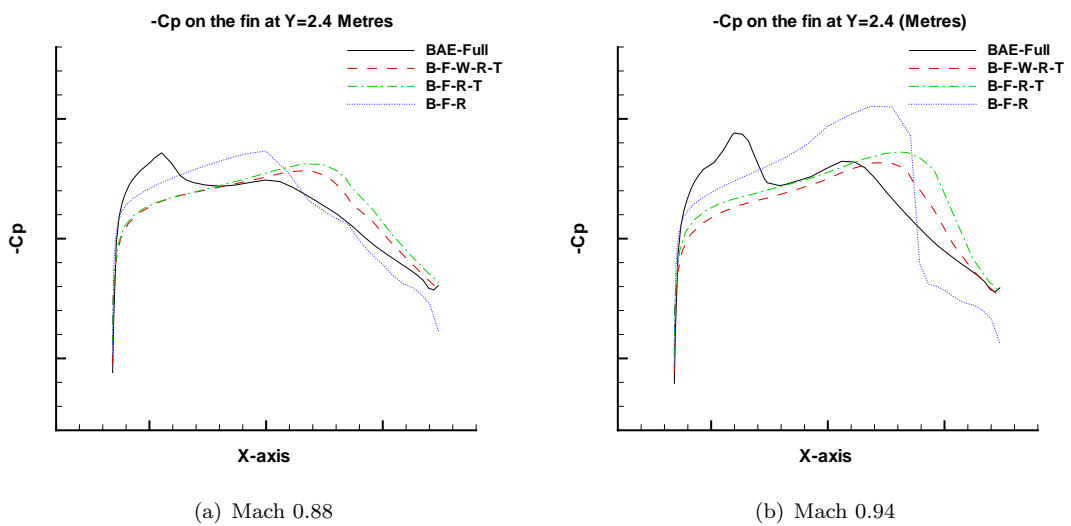


Figure 17. Surface pressure plots on the fin of the complete Hawk configuration at 2.4 Metres span

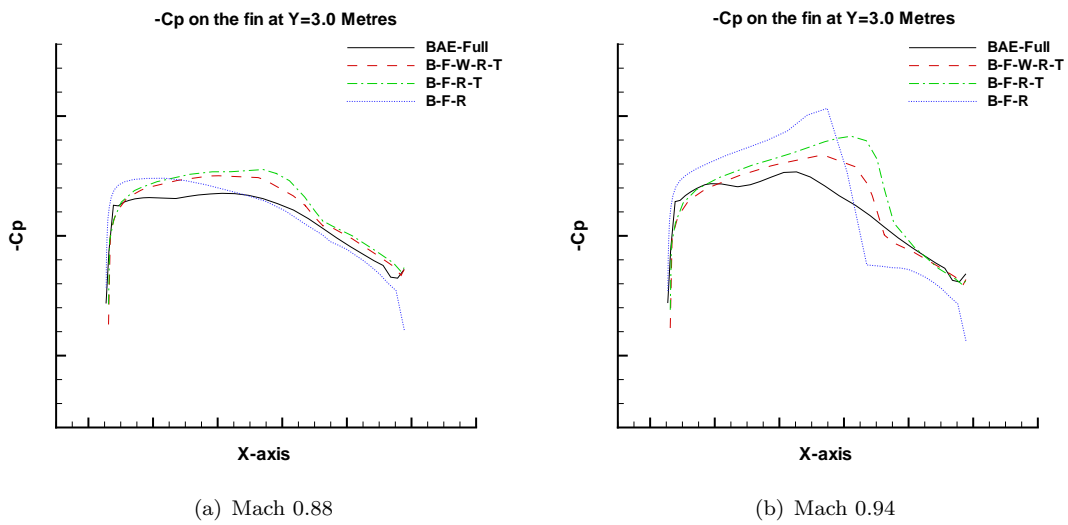


Figure 18. Surface pressure plots on the fin of the complete Hawk configuration at 3 Metres span

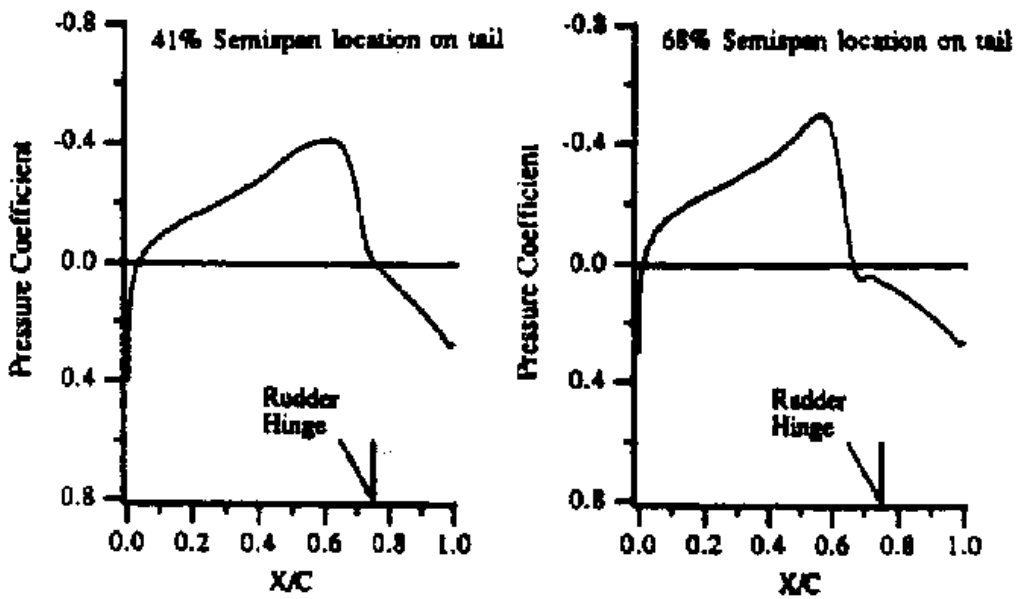
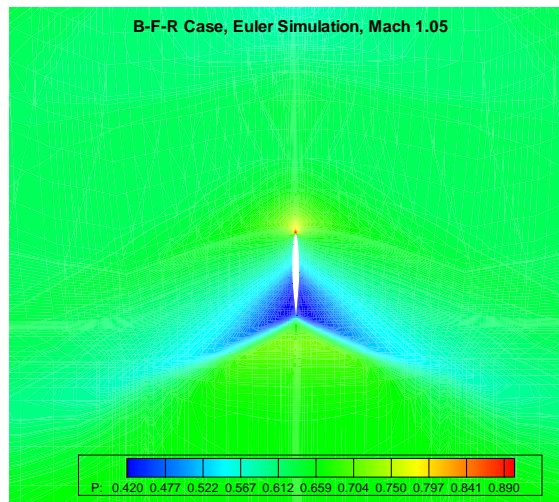
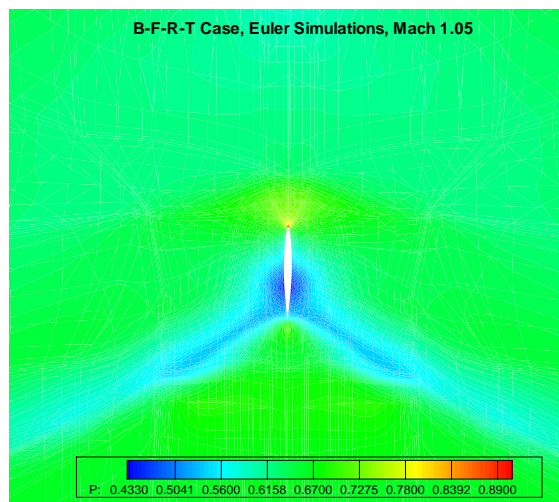


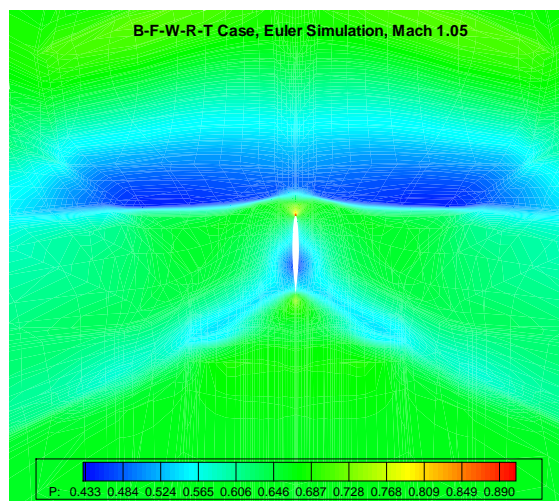
Figure 19. The surface pressure plots as predicted on the Goshawk in reference⁶ using RANS equations at Mach 0.95 and incidence 0° for the B-F-R case. Note that the tail in the title is referred to as the fin in this paper.



(a) The B-F-R case at Mach 1.05



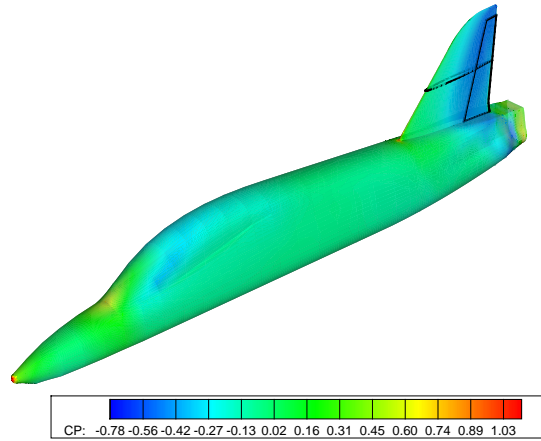
(b) The B-F-R-T case at Mach 1.05



(c) The B-F-W-R-T case at Mach 1.05

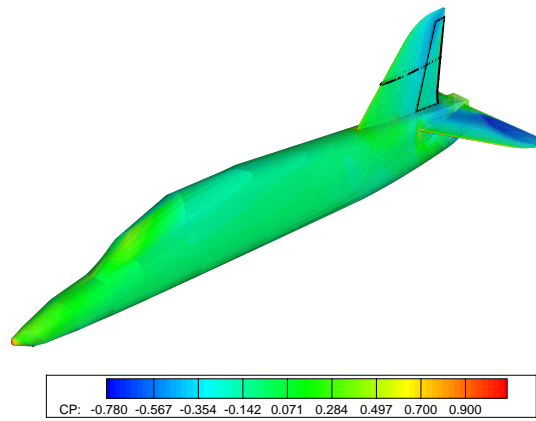
Figure 20. Hawk steady pressure contours at Mach 1.05 for increasing level of geometric complexity shows the gradual formation of shock ahead of the fin. The cases without the wing show a shock over the rudder.

B-F-R Case, Euler Simulation, Mach 1.05



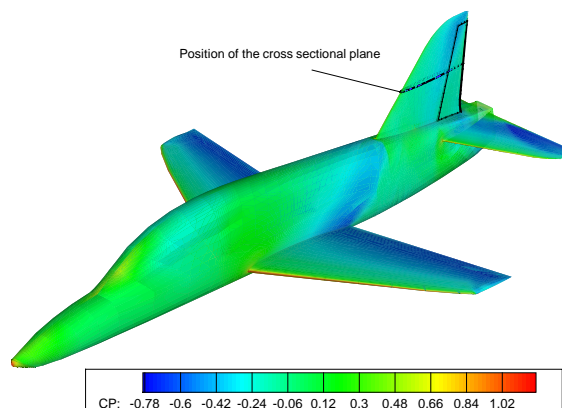
(a) The B-F-R case at Mach 1.05

B-F-R-T Case, Euler Simulation, Mach 1.05



(b) The B-F-R-T case at Mach 1.05

B-F-W-R-T Case, Euler Simulation, Mach 1.05



(c) The B-F-W-R-T case at Mach 1.05

Figure 21. Hawk steady surface pressure contours at Mach 1.05 for cases with increasing level of complexity. The shock over the wing alters the pressure distribution over the fin-rudder due to deceleration of the flow after the shock.

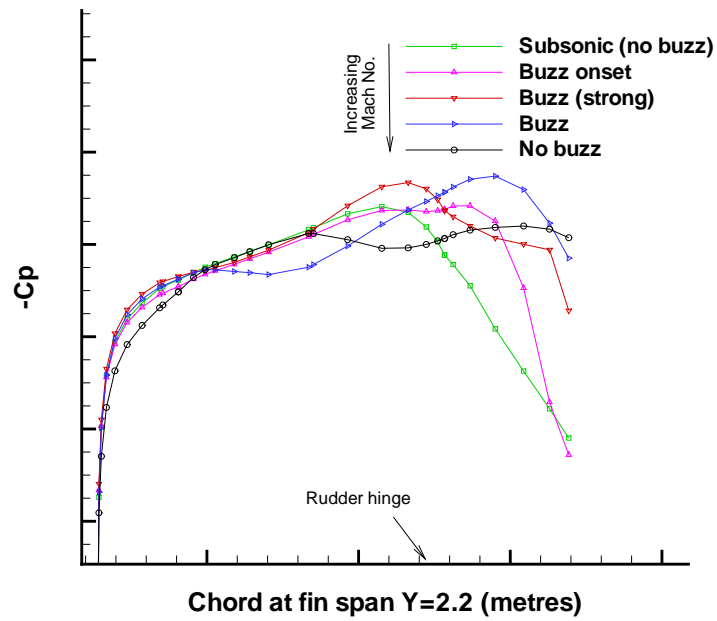


Figure 22. Cp plot at 2.2 metres fin span at increasing Mach numbers shows the strengthening and the gradual weakening of the shock across the fin span with for the Hawk B-F-W-R-T case. A region between transonic and lower supersonic Mach numbers exhibits buzz. .

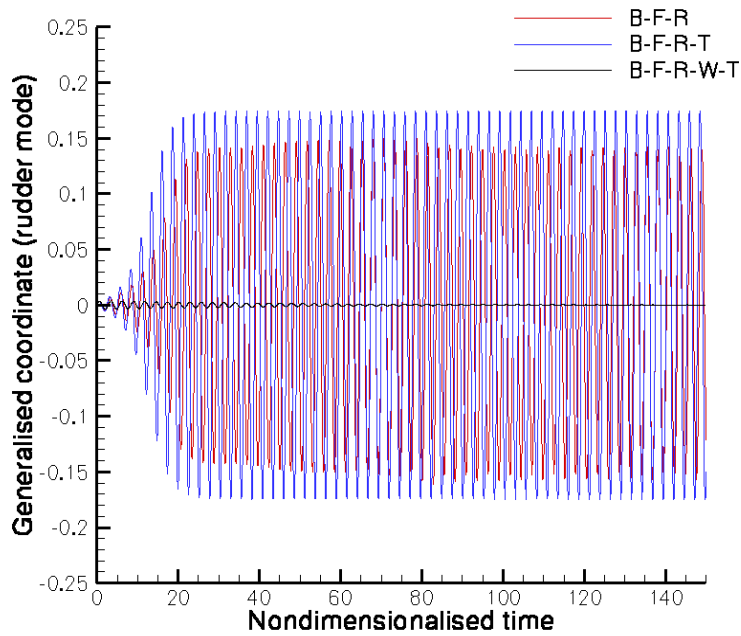


Figure 23. Modal response of the three Hawk cases at Mach 0.97 and dynamic pressure of 44.9 kPa.